Advances in Geosciences
Vol. 12: Ocean Science (2007)
Eds. Jianping Gan *et al.*

PROCESS-ORIENTED STUDY OF THE RIVER PLUME AND CIRCULATION IN THE PEARL RIVER ESTUARY: RESPONSE TO THE WIND AND TIDAL FORCING

TINGTING ZU
Atmospheric, Marine, Coastal Environment (AMCE) Program
Hong Kong University of Science and Technology
Clear Water Bay, Kowloon, Hong Kong

JIANPING GAN
Department of Mathematics
Hong Kong University of Science and Technology
Clear Water Bay, Kowloon, Hong Kong
magan@ust.hk

A three-dimensional, primitive equation numerical model is utilized to study the responses of the river plume and estuarine circulation to the wind and tidal forcing in an idealized Pearl River Estuary (PRE) with simplified geometry and physical forcing. This process-oriented study shows that without any other physical forcing, the buoyant-driven circulation, under the Earth rotation effect, forms an anticyclonic eddy in a funneled estuary with a concave bathymetry. However, this eddy disappears with additional wind or tidal forcing. The movement of the buoyant plume is retarded, and the thickness of the plume is largely increased by the tidal forcing as a result of the great enhancement of the vertical mixing inside the estuary and around the mouth of the estuary on the shelf. On the other hand, with wind forcing, the plume moves faster along the seaward branch of the wind-induced estuarine circulation with a narrower width confined by the current. And the wind-induced circulation increases the intrusion of the oceanic saltier water into the estuary, especially in upwelling case, and the consequently enhanced stratification along the axis of the estuary reduces the vertical mixing and the thickness of the plume. The study reveals the interactive roles of the buoyant plume, tidal, and wind forcing on the circulation in the estuary and adjacent shelf waters.

1. Introduction

Pearl River Estuary (PRE), which is also called Lingdingyang in Chinese, is located along the south coast of mainland China at 113.5°–114.1°E and 22°–22.8°N). It is the main estuary that connects Pearl River with the northern South China Sea (NSCS) continental shelf. The annual average total discharge of Pearl River is about 10,000 $\mathrm{m^3\,s^{-1}}$, of which more than half (about 5700 $\mathrm{m^3\,s^{-1}}$) flows into the PRE, and the ratio of maximum to minimum discharges in a year could vary by 3–6 times. Situated in the northern South China Sea (SCS), the PRE is under the influence of the East Asia Monsoon. Strong northeasterly wind (average wind speed of 7–10 $\mathrm{ms^{-1}}$) prevails in the winter, and much weaker (generally $<6\,\mathrm{ms^{-1}}$) southwesterly wind prevails in the summer. The PRE region is characterized as a micro-tidal coast with a tidal range about 1 m.[7,30] Considering all the factors stated above, it is not hard to reach the conclusion that the buoyant plume, estuarine circulation, and the flow field over the adjacent shelf might be greatly influenced by the variation of fresh water discharge, wind stress, and tidal mixing effects.

Previous studies on the plume and circulation in the PRE[7,30,34] showed that the elevation and salinity gradient are larger in the cross-estuary direction (normal to the axial direction) than those in the along-estuary direction (axial direction), and the plume front along the axial direction shows a characteristic of coastal front. They concluded that the classical gravitational circulation does not seem to be the principle mode of the circulation inside the PRE, especially in the lower half of the PRE, where the circulation assumes a typical pattern of a coastal current, and a transformation of the circulation pattern from a river plume to a coastal current exists in the middle reach. Unlike other normal estuaries, the PRE is so wide that it acts like a coastal sea for the river, namely, the coastal processes take effect inside the lower part of the estuary. They also found that the river plume and the related frontal zone vary with the changing monsoon wind and freshwater influx. During northeast monsoon (dry season), the plume is narrower than that in the wet season and flows out along the western estuary, while during the southwest monsoon (wet season), the plume is wide (usually dominant in the surface of the estuary), and its structure outside the estuary is much more diverse[26] due to the weaker and less steady southwest wind. By studying the tides and tidal currents in the PRE, Mao *et al.*[22] also pointed out that an anticlockwise circulation exists inside the estuary.

The estuarine circulation and associated river plume also play important roles in the biogeochemical processes in both estuary and shelf waters. Observation results around PRE show that the spatial variability of phytoplankton biomass and primary productivity are closely related to the structure and motion of the wind-controlled river plume.[37] Their results also showed that the estuarine circulation and stratification are important in determining the residence time of the bottom layer and consequently the dissolved oxygen in the bottom layer below the euphotic zone.[38] Both evidences reveal the fact that understanding the dynamic processes and related forcing mechanisms in the PRE as well as in the adjacent shelf is critical in interpreting the local biogeochemical processes.

There are many observational, analytical, and numerical model studies[1–4,6,11,12,15–17,19,20,31,33,35,36] of river plume and estuarine circulation regarding the effect of bathymetry, river discharge rate, wind stress, tidal mixing and coastal ambient current on the shape and motion of the plume, and the structure of the transverse circulation in estuaries. However, most of these studies, no matter real case study or idealized modeling, are for narrower estuaries (where the Coriolis effect is not that strong) with smaller river discharge (the buoyant force is not that strong) compared with the PRE. There are few numerical simulations or analyses of the responses of the river plume and estuarine circulation to the various types of physical forcing in PRE, not to mention the interaction between the coastal and estuarine dynamic processes there. In this study, we apply an idealized estuary–shelf coupled model system, representing the PRE and NSCS shelf, to study the responses of the plume, and coupled estuarine–coastal circulation to the buoyancy, tidal forcing, upwelling, and downwelling favorable winds. The advantage of this process-oriented numerical simulation is that the unknown processes induced by each of these physical forcings can be deterministically identified in the well-defined idealized simulations, and thus paves the way for the realistic simulations.

2. Model Implementation

The Regional Ocean Modeling System (ROMS),[27] which is a free-surface, stretched terrain-following, hydrostatic, primitive-equation ocean model, is utilized. The ROMS has been successfully implemented on the studies of river plume and estuarine circulation by MacCready and Geyer[21]; Hetland[17]; Warner *et al.*[32]; Choi and Wilkin.[6]

The model domain (Fig. 1) is a parallelogram, with a trapezoid estuary (representing the PRE) connecting to a parallelogram shelf (representing the NSCS coastal shelf). The estuary is approximately 61 km long and 59 km wide at the open mouth, and the shelf part of the domain is about 334 km long and 75 km wide. There are 340×160 horizontal grid points with corresponding resolution of about 983×874 m, 30 vertical

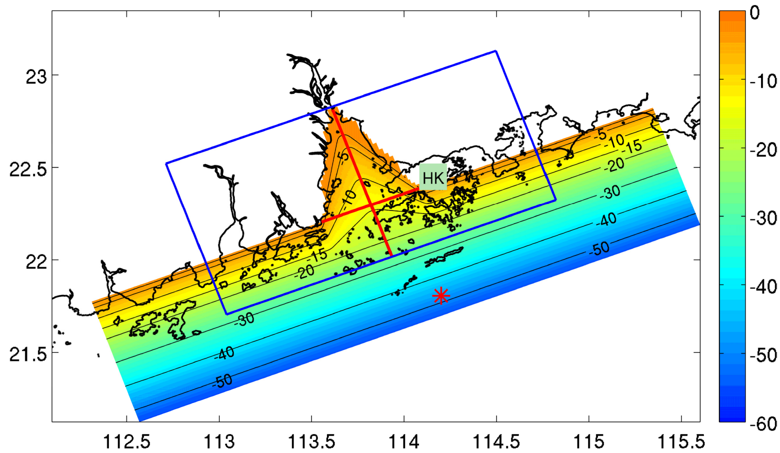

Fig. 1. Model domain and topography. Black contours are the coastlines of the northern South China Sea around the Pearl River Estuary. Color contours show the model domain and idealized topography. Model results inside the blue box and along the two sections (denoted by the red lines) will be shown in the following figures. The red asterisk shows the location of the observation station of the salinity and temperature profiles, and "HK" in the green box stands for Hong Kong.

s-level[29] with resolution varying from about 0.03 m in both surface and bottom boundary layers to 2.4 m in the interior of the water column. The higher horizontal and vertical resolutions are adopted in order to prevent the formation of wave-like meanders around the plume bulge, as mentioned by Berdeal *et al.*[1] Hyatt and Signell,[18] and Fong.[10] An idealized water depth, which is horizontally symmetric on the left and right sides of the estuary axis with a sloping bottom along the northwest–southeast direction, is utilized to mirror the real topography in the PRE and its adjacent coastal waters. Freshwater flux of about $5800\,\mathrm{m^3\,s^{-1}}$, representing the annual average river discharge rate into the PRE, is distributed uniformly in the entire water column at the uppermost estuary end and is ramped up over 3 days to prevent generating numerical shocks. The model is initialized with zero velocity and surface elevation, and with horizontally uniform initial salinity and temperature field obtained from the observation profile at a station (114.2°E, 21.806°N, Fig. 1) outside the mouth of PRE during summer. The water is almost well mixed in the upper 15 m, with temperature around 28.5°C and salinity around 33 psu, the temperature/salinity changes sharply at the thermocline/halocline at about 15–25 m, and below 25 m the temperature/salinity decreases/increases

Table 1. Summaries of the idealized cases.

	River discharge	Tidal forcing	Wind forcing	Earth rotation
Case 1	$5800\,m^3\,s^{-1}$	No	No	$f = 5.52 \times 10^{-5}$
Case 2	$5800\,m^3\,s^{-1}$	M_2 tide	No	$f = 5.52 \times 10^{-5}$
Case 3	$5800\,m^3\,s^{-1}$	No	Downwelling	$f = 5.52 \times 10^{-5}$
Case 4	$5800\,m^3\,s^{-1}$	No	Upwelling	$f = 5.52 \times 10^{-5}$
Case 5	$5800\,m^3\,s^{-1}$	No	No	$f = 0$

gradually to 22.7°C/34 psu. The spatially and temporally uniform upwelling favorable wind (representing summer monsoon) and downwelling favorable wind (representing winter monsoon) with a magnitude of 0.025 Pa are applied in the study respectively. Tidal harmonic constants of M_2 tide calculated from a SCS tidal model[39] are applied on the open boundary. Cyclic open boundary conditions are adopted in the alongshore direction, while Orlanski-type[24] radiation conditions are applied in the southern open boundary. In the case with tidal forcing, it is applied in the depth-average velocity field similar to that in the study by Flather.[9]

Like the previous findings,[1,8,18,40] our sensitivity study also shows that the central difference schemes for advection terms will introduce a numerical dispersion resulting in ripples and extremely high or negative salinity if the estuary is shallow and the river discharge is large. The Multidimensional Positive Definite Advection Transport Algorithm (MPDATA),[28] which uses an "anti-diffusion" velocity in a successive upwind scheme to iteratively correct first-order truncation errors, is chosen for solving the temperature and salinity equation, while the UPWIND scheme is adopted for the advection terms in momentum equations. The Mellor and Yamada[23] level 2.5 turbulent closure scheme is used to parametrize the vertical mixing.

We have conducted several simulations (Table 1) with different forcing schemes to identify the dominant forcing process in the region. Results from the five runs are presented and discussed in this paper. Case 1 is only with river discharge, and the effect of the tidal forcing with buoyant discharge is considered in case 2. Cases 3 and 4 are forced with additional (compared to case 1) upwelling and downwelling favorable wind, respectively. The effect of earth rotation is tested in case 5 with Coriolis force equal to zero.

3. Model Results

Results of the five cases, averaged over the 20th M_2 tidal cycle, are presented one by one in this section. For the convenience of comparison among these

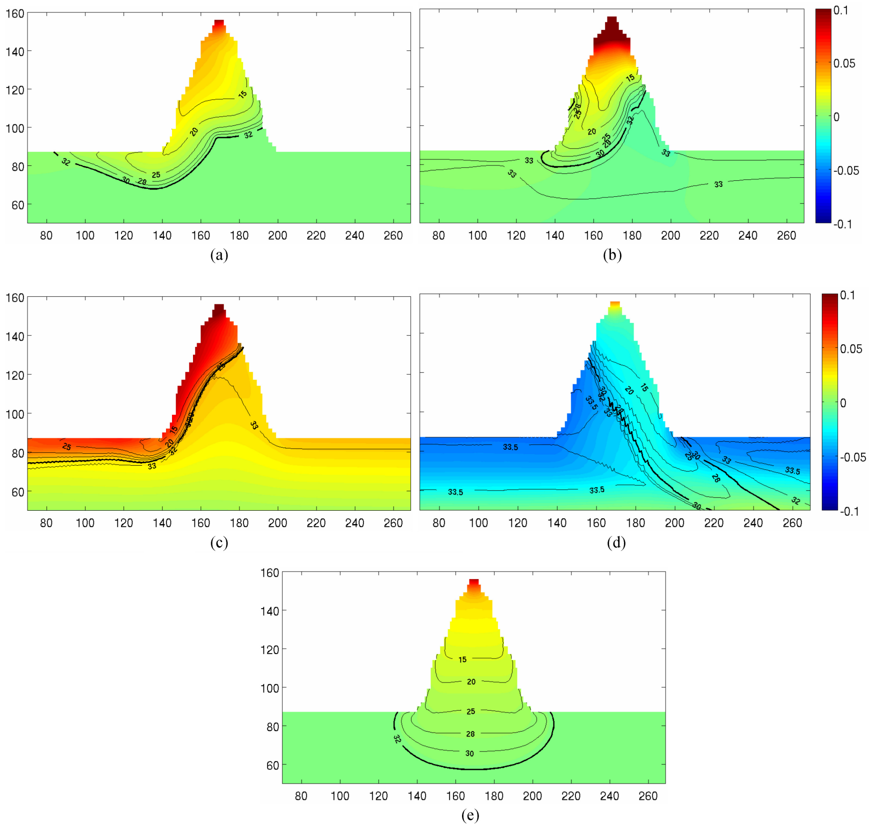

Fig. 2. Distribution of the salinity (black contour lines) and gradient of the sea surface elevation (m, color contour). The number along x- and y-axes denote the grid number. (a) is the base case, (b) is the case with tidal forcing, (c) and (d) are the cases with downwelling and upwelling favorable wind, respectively, and (e) is the case without the Coriolis effect ($f = 0$).

cases, the fields with same variables for the five cases are grouped together in each individual figure. The horizontal structures of the buoyant plume and circulation patterns inside the blue box (Fig. 1) are presented in Figs. 2 and 3. The plume structure and current fields in the vertical section along the axial direction of the PRE are given in Figs. 4 and 5. The flow fields along the vertical section across the PRE mouth are shown in Fig. 6. The isohaline of 32 psu is treated as the outer boundary of the buoyant plume in Figs. 2 and 4.

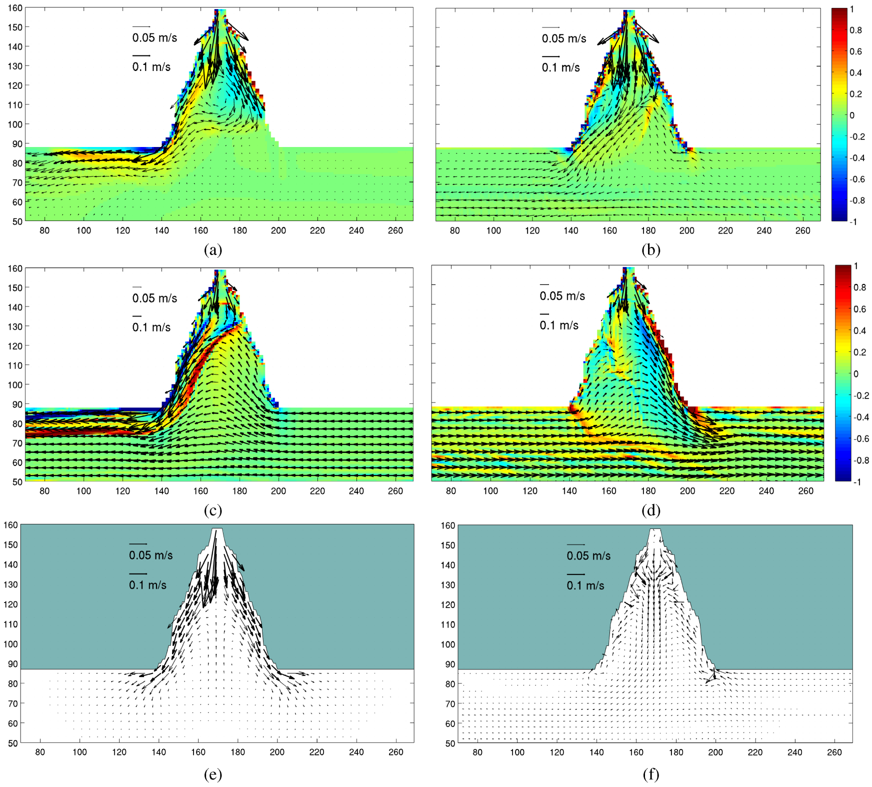

Fig. 3. Distribution of the barotropic current field and the ratio of relative vorticity to planetary vorticity $\frac{\varsigma}{f}$ (color contours). The sequence of the first five pictures is the same as that in Fig. 2. Picture (f) is the purely M_2 tidal residual current.

3.1. *River-forced buoyant plume and estuarine circulation (case 1)*

In case 1, buoyancy of the Pearl River discharge is the only mechanism that drives the estuarine circulation. Figure 2(a) shows that the freshwater plume almost dominates the whole surface of the estuary except the eastern part at the estuary mouth. The inclination of the sea surface follows the shape of the buoyant plume with higher elevation at the northwestern part of the estuary. The plume moves southward in the estuary and westward after entering the shelf. A bulge of freshwater plume is formed at the salient edge on the western side of the estuary entrance. Two strong currents exist along the western and eastern coast of the estuary while an anticyclonic

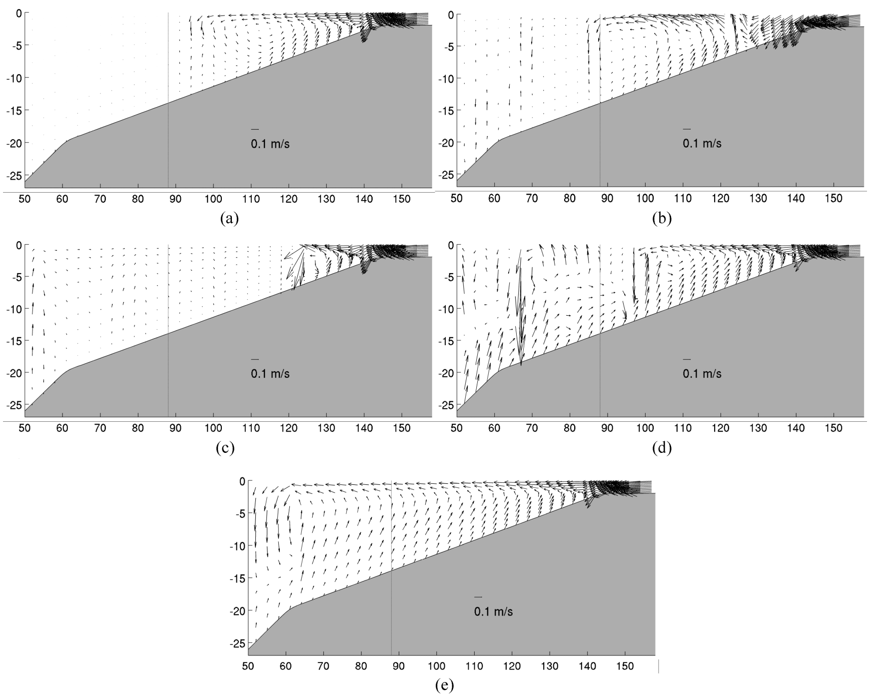

Fig. 4. Current field along the axial vertical section. Vertical velocity vector w is multiplied by 0.5×10^4 before plotting. The x-axis denotes the grid number in the horizontal y-direction, and the y-axis denotes the water depth. The red line shows the location of the estuary mouth. The sequence of the five pictures is the same as that in Fig. 2.

circulation is embedded in between (Fig. 3(a)). The jet on the eastern coast turns westward in the lower estuary and forms this anticyclonic circulation in the central part of the estuary. Part of this westward turning jet joins the jet along the west coast and forms a strong westward coastal current over the shelf, in the direction of the propagation of coastal-trapped Kelvin wave. Previous numerical studies[2,4,15,36] forced solely by river discharge also showed the similar characteristics of plume motion and coastal jet, but much larger bulge is formed on the shelf when the plume is surface-advected and the Coriolis force is strong, whereas, none documented an anticyclonic eddy inside the estuary. We speculate that the wide funneled shape and the concave bathymetry in the PRE are responsible for the formation of this eddy. And, the PRE acts much more like a coastal region rather than an estuary.

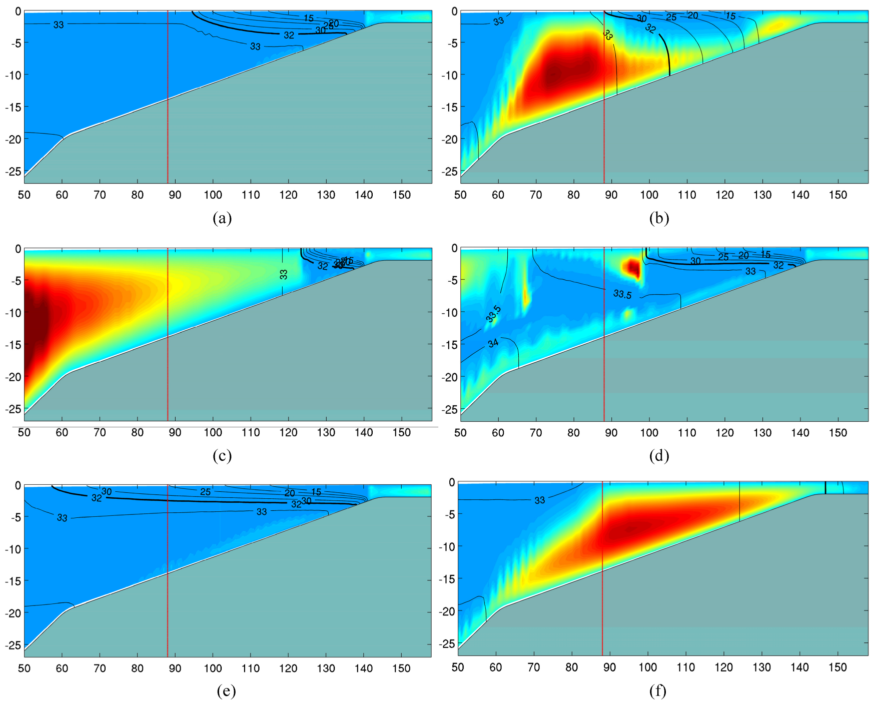

Fig. 5. Contours of the averaged salinity and AK_v on the vertical section along the axial of the PRE. The x-axis denotes the grid number in the horizontal y-direction, and the y-axis denotes the water depth. The red line shows the location of the estuary mouth. The sequence of the first five pictures is the same as that in Fig. 2, and they are all averaged in the 20th M_2 tidal cycle. Picture (f) is the same case as (b), but it is averaged in the 4th M_2 tidal cycle.

Along the axial vertical section, the isohaline contours show a surface-trapped river plume advancing seaward. It detaches from the bottom about 19 km from the estuary head (Fig. 4(a)). A classical two-layered estuarine circulation, with seaward outflow in the upper layer and landward inflow in the bottom layer, is shown in Fig. 5(a). With the downward motion at the head of the plume front, a counter-clockwise circulation, viewing with estuary head on the right-hand side, is formed in the meridional direction. The downward motion at the plume front, as a result of surface convergence was also found by Chao[2] and O' Donnell *et al.*[25] The prominent characteristic of current field on the vertical transverse section at the river mouth is that the two-layered flow occurs mainly on the west side of the estuary, with thinner layer (<5 m) of outflow and thick layer of inflow

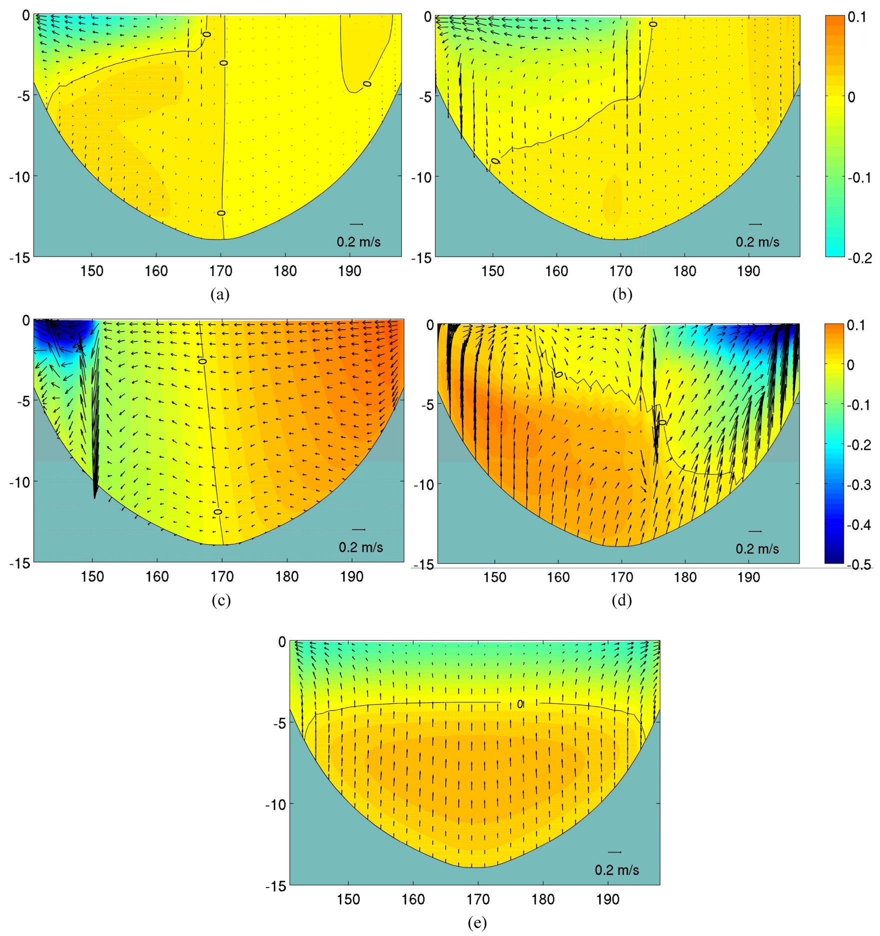

Fig. 6. Landward view of the averaged current field in the 20th M_2 tidal cycle along the vertical section at the mouth of PRE. Color contour shows the axial velocity vector $\mathbf{v}$. Vertical velocity vector $\mathbf{w}$ is multiplied by 0.5×10^4 before plotting. The sequence of the five pictures is the same as that in Fig. 2.

(Fig. 6(a)). In addition, the strong westward current is confined to the upper 5 m.

3.2. *Effects of tidal forcing (case 2)*

The structures of the plume and current field are greatly modified by adding the tidal forcing in the simulation in case 2. The seaward movement of the plume is deterred by the tidal forcing, and the head of the plume is located in a much shoreward position at the entrance of the estuary (Fig. 2(b)) as compared to case 1. More saline water occupies the eastern part of the estuary and the shelf near the coast. Freshwater piles up at the head of PRE and generates a larger axial pressure gradient as the plume intrusion speed slows down. Similar to case 1, the orientation of the gradient of the sea surface elevation largely follows the isohaline contours, indicating the control of buoyancy on the pressure field. For the horizontal current field, the anticyclonic circulation inside the estuary and the two jets along the eastern and western coasts of the estuary in case 1 disappear. They are replaced by strong southward currents in the upper part of the estuary and the southwestward currents as the entrance of the estuary is approaching (Fig. 3(b)). The change of the circulation is also related to the tidal residual current field shown in Fig. 3(f). The M_2 tidal residual currents flow into the estuary along the two shoulders with eastern current stronger than the western, and flow out mainly along the middle axial. These lead to the formation of a clockwise and a counter-clockwise circulation in the western and eastern sides of the estuary, respectively, similar to the pair of eddies caused by tidal residual currents outside the estuary mouth as described by Chao.[5] Again, the phenomenon supports the viewpoint that the PRE acts like a coastal region rather than an estuary. The stronger intrusion residual current on the eastern shoulder together with the right turning effect of the Coriolis force on the freshwater plume in the northern hemisphere make the eastern side of the estuarine water more oceanic.

Along the axial section (Fig. 4(b)), the plume in case 2 becomes more barotropic in which the entire freshwater column advances seaward in the upper estuary. The detachment occurs further seaward in this case, and the intensity of salinity front is weaker as compared to case 1. As shown in Figs. 4(b) and 4(f), the vertical mixing coefficient AK_v is greatly increased inside the estuary and, in particular, around the outer part of the estuary mouth after tidal forcing is included. Figure 4(f) shows the results averaged in the 4th M_2 tidal cycle when the plume has not formed in the estuary yet. The difference clearly suggests that the plume tends to suppress the vertical mixing. When plume propagates outward, the increased buoyancy shuts down the vertical mixing in the upper layer inside the estuary (Fig. 4(b)). However, the instability and enhanced vertical motion at the plume front make the strongest vertical mixing appear near the front, outside the PRE mouth. The axial circulation of the estuary (Fig. 5(b)) is similar to that in case 1, but appears to be enhanced with tidal outflow/inflow in the upper/lower layer, which leads to a stronger meridional circulation in the axial direction. The stronger downward motion at the head of the

PRE is probably due to the convergence of the discharged water when the movement of the river plume is slowed down, as also shown by the increased surface tilt in Fig. 2(b). Compared to case 1, the vertical motion is also increased on the coastal shelf (Fig. 6(b)), which will potentially affect the physical environment around the plume by bringing denser seawater upward. Despite that the outflow is still on the western coast of the estuary, it is wider and thicker as compared to case 1. The strongest inflow occupies the eastern part of the section instead of lower western coast as in case 1. The enhanced downward motions at the middle axial and western coast are obvious.

3.3. *Wind effects (cases 3 and 4)*

Effects from wind forcing are examined in cases 3 and 4, by running with downwelling (northeasterly) and upwelling (southwesterly) favorable wind stress, respectively. From Fig. 2(c), we could find that the freshwater is confined along the western coast of the estuary as a slim plume which moves westward after leaving the estuary during downwelling. Thus, most part of the estuary is dominated by the oceanic water. The sea surface tilts in the northwest–southeast direction in the estuary and in the north–south over the adjacent shelf west of the estuary. The co-effect of the river buoyancy and the surface Ekman transport account for the higher elevation inside the plume and over the inner shelf. Contrarily, in the upwelling case (Fig. 2(d)), the plume is confined in a strip along the eastern coast, and it is wider than that in the downwelling case. The buoyant plume moves southeastward after leaving the estuary instead of moving along the eastern coast as a "coastal-trapped" type. The saltier oceanic water occupies the southwestern part of the estuary, and the negative sea surface elevation is caused by the southward Ekman transport induced by the upwelling favorable wind. It seems that the changes of the structure and the motion of the plume are closely correlated with the coastal and estuarine circulation, as shown in Figs. 3(c) and 3(d). Strong westward/eastward current is formed along the shelf with an unclosed counter-clockwise/clockwise circulation near the entrance of the estuary during the downwelling/upwelling case. Much stronger westward coastal currents induced by the larger cross-coast pressure gradient as a result of both the buoyancy and the Ekman transport effects, occur in the downwelling case. Accordingly, the intrusion of the coastal current into the estuary tends to be stronger in the downwelling case.

Along the axial vertical section, a two-layer buoyancy-driven circulation exists only at the upper reach of the PRE in case 3 (Figs. 4(c) and 5(c)) during the downwelling, since the plume is closely confined to the western side of the estuary. The vertical mixing is increased both in the estuary and over the shelf, which is, however, different from that of the tidal mixing. The strongest mixing in case 3 occurs on the coast other than in the estuary. In case 4, during the upwelling period, the landward and upward currents occur in the bottom layer (Fig. 5(d)) over the entire estuary. The intrusion of the coastal deeper water brings saltier oceanic water upward and landward into the estuary from the adjacent shelf. It enhances the vertical salinity gradient (Fig. 4(d)) in the estuary and makes it a salt wedge estuary. The increasing stratification thus weakens the vertical mixing in the estuary. Unlike case 3, the vertical mixing in case 4 is only obvious in the surface and bottom layer, and the thickness of the plume is reduced to only about 2.5 m. The plume detaches from the bottom at about 17.5 km away from the river end, nearer to the estuary entrance than that in cases 1, 2, and 3. The magnitude of the inflow/outflow through vertical section along the line across the entrance of the estuary is much stronger as compared to no-wind cases, suggesting the importance of the wind-driven shelf circulation on the net water exchange between the estuary and the shelf. In the downwelling case (Fig. 6(c)), the freshwater flows out on the western side of the estuary, and the saltier water flows in on the eastern side. On the whole, the westward currents across the estuary behave like coastal current (Su, 2004). However, the transverse circulation for the upwelling case (Fig. 6(d)) is much more complicated. The plume becomes wider and thinner, with inflow at the western coast and at the bottom while the outflow at the upper eastern coast. Strong upward motions occur on both sides at the entrance, with a downward motion in between.

4. Discussion

As presented in Sec. 3, the estuarine circulation and the characteristics of the associated buoyant plume are greatly controlled by the physical processes induced by the tidal and wind forcing. To facilitate further investigation of the relative importance of earth rotation, current, and the purely gravitational effect, on the plume, an additional case (case 5) similar to case 1 but with Coriolis parameter f set to zero, is conducted.

Without earth rotation and other types of external forcing, the plume moves southward with a symmetrical classical two-layer gravitational circulation and a big fresh water bulge is formed outside the mouth (Figs. 2(e), 3(e), 4(e), 5(e), and 6(e)). The sea surface elevation and isohaline mirror each other with strong gradients in the north–south direction. Two branches of strong jet form along both shoulders of the estuary, with a much weaker inflow along the middle axial (Fig. 3(e)). This current pattern is different from that in case 1, in which the current of the eastern branch is shifted westward and forms a clockwise circulation inside the estuary (Fig. 3(a)). By comparing the structures of isohaline and estuarine circulation among different cases in Figs. 2 and 3, it is apparent that the motion and shape of the plume are highly controlled by the currents and circulation, which have much stronger coastal instead of estuarine characteristics.

The distribution of the ratio of relative vorticity to planetary vorticity, $\frac{\varsigma}{f}$, the same as Rossby number but better representing the nonlinearity in the shear flow, in Fig. 3 shows, as expected, that the Coriolis term is more important than the advection term in both estuary and shelf, except at the slender plume boundary in downwelling case, where the current is highly nonlinear.

The structure of the plume is sensitive to the vertical mixing processes, as we can see that the thickness of the plume and the place it detaches from the bottom change in different situations (Fig. 4). The plume developed without Coriolis force (case 5) is thinner than that with Coriolis force (case 1), likely due to the absence of the convergent motion caused by the anticyclonic eddy inside the estuary in case 1. The tidal mixing increases the vertical mixing in the whole water column and forms vertically unstratified waters in the regions inside the estuary and on the shelf (Figs. 4(b) and 4(f)) until it is weakened by the highly stratified plume. However, in the upwelling case, the vertical mixing is also increased, but the plume is thinned, and detaches the bottom soon. One possible reason is that the vertical mixing is only increased in the surface and bottom boundary layers, and the stratified middle layer is hard to be well-mixed. What is more, the upwelled saltier water also intrudes into the estuary in the bottom layer, thus enhances the stratification and reduces the vertical mixing process.

5. Summary

By using a 3D numerical model, we have studied the responses of the river plume and estuarine circulation to the tidal and wind forcing in an idealized Pearl River Estuary. This process-oriented study shows that the PRE is characterized more by the coastal circulation than by the classical estuarine circulation driven by gravitational forcing. The plume-induced buoyant jet develops an anticyclonic eddy inside the PRE under both the gravitational and Coriolis forcing, and moves westward after leaving the estuary. Physical forcing from the tide and wind destroys the eddy and leads to the respective current field. In general, the tidal mixing acts to retard the seaward motion of the buoyant plume, whereas the wind forcing favors the movement but narrows the plume. The two-layer gravitational circulation is developed and modulated by the external forcing along the estuary direction in all cases but with different strengths and ranges.

The vertical structure of the plume is sensitive to the vertical mixing. With enhanced vertical mixing in the tidal case, the plume is greatly thickened and moves farther seaward before detaching from the bottom. And it suggests that the tidal forcing should have effect beyond the tidal frequency domain. Furthermore, the current fields on the transverse section at the estuary mouth show that the inflow/outflow pattern also changes dramatically from a lower–upper structure into an almost right–left structure when the external forcing is added, and this shift might have strong influence on the distribution of the oceanic and freshwater inside the estuary. Besides, one thing important to note is that the intrusion of the upwelled saltier water in the upwelling case enhances the stratification, and thus reduces the vertical mixing, and thins the plume. It is evident that the coastal processes do affect the estuarine processes. Therefore, shelf regions should be included in the whole model domain when the estuarine circulation is simulated. This simplified model study helps us to figure out the responses of the river plume and estuarine circulation to different physical forcing, and paves the road to more complicated real case simulations.

Nevertheless, there are still many more to be explored, for example, by increasing/decreasing the river discharge, changing the salinity influx of the river discharge, adding tide and wind forcing together to see their co-effect, and forcing with temporally changing wind stress, and so on. These studies are still under investigation, and will be presented in the future work.

Acknowledgments

This research was supported by the Research Grants Council of Hong Kong under Grants CERG-601105 and CERG-613007.

References

1. G. I. Berdeal, B. M. Hickey and M. Kawase, Influence of wind stress and ambient flow on high discharge river plume, *J. Geophys. Res.* **107**(C9) (2002) 3130, doi:10.1029/2001JC000932.
2. S.-Y. Chao, River-forced estuarine plumes, *J. Phys. Oceanogr.* **18** (1988) 72–88.
3. S.-Y. Chao, Wind-driven motion of estuarine plumes, *J. Phys. Oceanogr.* **18** (1988) 1144–1166.
4. S.-Y. Chao and W. C. Boicourt, Onset of estuarine plumes, *J. Phys. Oceanogr.* **16** (1986) 2137–2149.
5. S.-Y. Chao, Tidal modulation of estuarine plumes, *J. Phys. Oceanogr.* **20** (1990) 1115–1123.
6. B. Choi and J. L. Wilkin, The effect of wind on the dispersal of the Hudson River plume, *J. Phys. Oceanogr.* **37** (2007) 1878–1897.
7. L. X. Dong, J. L. Su, L. A. Wong, Z. Y. Cao and J. C. Chen, Seasonal variation and dynamics in the Pearl River plume, *Continental Shelf Res.* **24** (2004) 1761–1777.
8. W. Fennel and A. Mutzke, The initial evolution of a buoyant plume, *J. Marine Syst.* **12** (1997) 53–68.
9. R. A. Flather, A tidal model of the north-west European continental shelf, *Mem. Soc. R. Sci. Liège* **6**(10) (1976) 141–164.
10. D. A. Fong, Dynamics of freshwater plumes: Observations and numerical modeling of the wind-forced response and along-shore freshwater transport, PhD thesis, MIT/WHOI Joint Program in Oceanography, Woods Hole, Mass. (1998).
11. D. A. Fong and W. R. Geyer, The alongshore transport of freshwater in a surface-trapped river plume, *J. Phys. Oceanogr.* **32** (2001) 957–972.
12. D. A. Fong and W. R. Geyer, Response of a river plume during an upwelling favorable wind event, *J. Geophys. Res.* **106**(C1) (2001) 1067–1084.
13. P. J. S. Franks and D. M. Anderson, Alongshore transport of a toxic phytoplankton bloom in a buoyancy current: *Alexandrium tamarense* in the Gulf of Maine, *Marine Biol.* **112** (1992) 153–164.
14. I. Garcia-Berdeal, B. M. Hickey and M. Kawase, Influence of wind stress and ambient flow on a high discharge river plume, *J. Geophys. Res.* **107**(C9) (2002) 3130.
15. R. W. Garvine, Penetration of buoyant coastal discharge onto the continental shelf: A numerical model experiment, *J. Phys. Oceanogr.* **29** (1999) 1892–1909.
16. X. Guo and A. Valle-Levinson, Tidal effects on estuarine circulation and outflow plume in the Chesapeake Bay, *Continental Shelf Res.* **27** (2007) 20–42.
17. R. D. Hetland, Relating river plume structure to vertical mixing, *J. Phys. Oceanogr.* **35** (2005) 1667–1688.
18. J. Hyatt and R. P. Signell, Modeling surface trapped river plumes: A sensitivity study, *in Estuarine and Coastal Modeling, 6th Int. Conf.*,

(eds.) M. L. Spaulding and A. F. Blumberg, ASCE, New Orleans, LA, 3–5, November 1999.

19. A. Kasai, A. E. Hill, T. Fujiwara and J. H. Simpson, Effect of the Earth's rotation on the circulation in regions of freshwater influence, *J. Geophys. Res.* **105** (2000) 16961–16969.
20. P. MacCready, Estuarine adjustment to changes in river flow and tidal mixing, *J. Phys. Oceanogr.* **29** (1999) 708–729.
21. P. MacCready and W. R. Geyer, Estuarine salt flux through an isohaline surface, *J. Geophys. Res.* **106** (2001) 11,629–11,637.
22. Q. Mao, P. Shi, K. Yin, J. Gan and Y. Qi, Seasonal variation and dynamics in the Pearl River plume, *Continental Shelf Res.* **24** (2004) 1797–1808.
23. G. L. Mellor and T. Yamada, Developement of a turbulence closure model for geophysical fluid problems, *Rev. Geophys. Space Phys.* **20** (1982) 851–875.
24. I. Orlanski, A simple boundary condition for unbounded hyperbolic flows, *J. Comput. Phys.* **21** (1976) 251–269.
25. O' Donnell *et al.*, Convergence and downwelling at a River Plume Front, *J. Phys. Oceanogr.* **28** (1998) 1481–1495.
26. S. Ou, H. Zhang, D. Wang and J. He, Horizontal characteristics of buoyant plume off the Pearl River Estuary during summer, in *SI 50 Proc. 9th International Coastal Symposium*, Gold Coast, Australia, ISSN 0749.0208, pp. 652–657.
27. A. F. Shchepetkin and J. C. McWilliams, The regional ocean modeling system: A split-explicit, free-surface, topography following coordinates ocean model, *Ocean Modelling* **9** (2005) 347–404.
28. P. K. Smolarkiewicz, A fully multidimensional positive definite advection transport algorithm with small implicit diffusion, *J. Computat. Phys.* **54** (1984) 325–362.
29. Y. Song and D. B. Haidvogel, A semi-implicit ocean circulation model using a generalized topography-following coordinate system, *J. Computat. Phys.* **115**(1) (1994) 228–244.
30. J. Su, Overview of the South China Sea circulation and its influence on the coastal physical oceanography outside the Pearl River Estuary, *Continental Shelf Res.* **24** (2004) 1745–1760.
31. A. Valle-Levinson, C. Reyes and R. Sanay, Effects of bathymetry, friction, and rotation on estuary–ocean exchange, *J. Phys. Oceanogr.* **33** (2003) 2375–2393.
32. J. C. Warner, W. R. Geyer and J. A. Lerczak, Numerical modeling of an estuary: A comprehensive skill assessment, *J. Geophys. Res.* **110** (2005) C05001.
33. M. M. Whitney and R. W. Garvine, Wind influence on a coastal buoyant outflow, *J. Geophys. Res.* **110** (2005) C03014, doi:10.1029/2003JC002261.
34. L. A. Wong, J. C. Chen and L. X. Dong, A model study of the plume front of the Pearl River Estuary, China and adjacent coastal waters in the winter dry season, *Continental Shelf Res.* **24** (2004) 1779–1795.
35. K.-C. Wong, On the nature of transverse variability in a coastal plain estuary, *J. Geophys. Res.* **99** (1994) 14209–14222.

36. A. E. Yankovsky and D. C. Chapman, A simple theory for the fate of buoyant coastal discharge, *J. Phys. Oceanogr.* **27** (1997) 1386–1401.
37. K. Yin, J. Zhang and P. Y. Qian, Effect of wind events on phytoplankton blooms in the Pearl River estuary during summer, *Continental Shelf Res.* **24** (2004) 1909–1923.
38. K. Yin, Z. Lin and Z. Ke, Temporal and spatial distribution of dissolved oxygen in the Pearl River Estuary and adjacent coastal waters, *Continental Shelf Res.* **24** (2004) 1935–1948.
39. T. Zu, J. Gan and S. Y. Erofeeva, Numerical study of the tide and tidal dynamics in the South China Sea, *Deep-Sea Res. I* **55** (2008) 137–154.
40. L. Zheng and R. H. Weisberg, Tide, buoyancy, and wind-driven circulation of the Charlotte Harbor estuary: A model study, *J. Geophys. Res.* **109** (2004) C06011, doi:10.1029/2003JC001996.